

# On the origin of star-formation quenching in massive galaxies at $z \gtrsim 3$ in the cosmological simulations IllustrisTNG

Shalini Kurinchi-Vendhan,<sup>1,2</sup>  Marion Farcy,<sup>3</sup> Michaela Hirschmann,<sup>3,4</sup> Francesco Valentino<sup>5,6</sup>

<sup>1</sup> *California Institute of Technology (Caltech), 1200 E. California Boulevard, Pasadena, California 91125, United States of America*

<sup>2</sup> *Max-Planck-Institut für Astronomie (MPIA), Königstuhl 17, Heidelberg 69117, Baden-Württemberg, Germany*

<sup>3</sup> *École Polytechnique Fédérale de Lausanne (EPFL), Observatoire de Sauverny, Chemin Pegasi 51, 1290 Versoix, Switzerland*

<sup>4</sup> *Istituto Nazionale di Astrofisica (INAF), Osservatorio Astronomico di Trieste, Via Tiepolo 11, 34131 Trieste, Italy*

<sup>5</sup> *European Southern Observatory (ESO), Karl-Schwarzschild-Strasse 2, D-85748, Garching bei München, Germany*

<sup>6</sup> *Cosmic Dawn Center (DAWN), Niels Bohr Institute, Rådmandsgade 62-64, 2200 Copenhagen, Denmark*

Accepted 2024 September 30. Received 2024 September 26; in original form 2023 October 2

## ABSTRACT

Using the cosmological simulations IllustrisTNG, we perform a comprehensive analysis of quiescent, massive galaxies at  $z \gtrsim 3$ . The goal is to understand what suppresses their star formation so early in cosmic time, and how other similar mass galaxies remain highly star-forming. As a first-order result, the simulations are able to produce massive, quiescent galaxies in this high-redshift regime. We find that active galactic nuclei (AGN) feedback is the primary cause of halting star formation in early, massive galaxies. Not only do the central, supermassive black holes (SMBHs) of the quenched galaxies have earlier seed times, but they also grow faster than in star-forming galaxies. As a result, the quenched galaxies are exposed to AGN feedback for longer, and experience the kinetic, jet mode of the AGN feedback earlier than the star-forming galaxies. The release of kinetic energy reduces inflows of gas while likely maintaining outflows, which keeps a low cold gas fraction and decreases the star formation of the galaxies down to a state of quiescence. In addition to AGN feedback, we also investigate the influence of the large-scale environment. While mergers do not play a significant role in the quenching process, the quenched galaxies tend to reside in more massive halos and denser regions during their evolution. As this provides a greater initial amount of infalling gas to the galaxies, the large-scale environment can mildly affect the fate of the central SMBH growth and, via AGN feedback, contribute to star formation quenching.

**Key words:** galaxies: formation – galaxies: evolution – galaxies: active – galaxies: high-redshift – methods: numerical

## 1 INTRODUCTION

Exploring how star-forming galaxies are converted into passive, or *quenched*, galaxies is fundamental to our understanding of galaxy evolution. The majority of massive galaxies become “red and dead” over cosmic time, but the continuous discovery of massive quenched galaxies at increasingly high-redshift remains puzzling (e.g. Long et al. 2023). Some physical mechanisms may prevent gas from being accreted onto the galaxy, keep gas in the galaxies from cooling and condensing, or expel gas from the galaxies. Together, these processes can deplete galaxies of their star-forming gas and eventually shut down star formation. We provide a brief overview of different possible quenching mechanisms in this introduction (see e.g. Man & Belli 2018).

To sustain star formation, the gas reservoir of a galaxy has to be regularly replenished by accretion from cosmic filaments or through merger interactions with gas-rich companions. When a galaxy accretes gas at an insufficient rate, this may eventually lead to cosmological starvation (Wetzel et al. 2013): the galaxy runs out of fuel and cannot form stars. Furthermore, the accreted gas needs to reach the interstellar medium (ISM) of the galaxy, which might be prevented

if gas cannot cool onto it. This can initially occur when virial shocks contribute to heating the gas. Gravitational interactions with satellites, which lead to dynamical friction, may also provide the energy needed for increasing the temperature of the gas (Rees & Ostriker 1977; Khochfar & Ostriker 2008).

Once the gas reaches the ISM, a history of “bursty” star formation and major mergers can facilitate the rapid loss of cold gas (Mihos & Hernquist 1996). To a lesser extent, and in addition to rapid star formation, active galactic nuclei (AGN) can consume cold gas through accretion onto supermassive black holes (SMBHs), eventually depleting the galaxy of part of its star-forming fuel. The suppression of star formation activity is not only connected to the gas reservoir but also depends on its ability to be converted into stars. In other words, galaxies can quench when their gas does not cool. While virial shocks and interactions with neighbouring galaxies can temporarily stop gas from falling towards the galaxies, additional mechanisms are required to prevent gas that reached the interstellar medium (ISM) from cooling and condensing to form stars. Stellar feedback from radiation, winds, and supernovae can lead to temporary shock-heating (Ciotti et al. 1991; Springel & Hernquist 2003), but is also very likely to be inefficient in maintaining quiescence in massive galaxies (e.g. Dubois et al. 2016; Choi et al. 2018). Instead, it is largely thought that sustained heating is driven by radiatively inefficient accretion

\* E-mail: skurinchi@caltech.edu

onto AGN (Bower et al. 2006; Croton et al. 2006): SMBHs accreting at a low rate produce jets that inflate buoyant bubbles of gas, heating the hot halo gas (Fabian 2012).<sup>1</sup> Other forms of feedback can also play an important role in clearing out the gas and quenching galaxies in the first place.

If gas is not prevented from cooling or condensing, a galaxy must expel part of its reservoir of cold gas faster than it can be replenished in order to remain quenched. Through near encounters with surrounding galaxies in a dense environment, low-mass galaxies can lose their star-forming gas content through processes such as ram-pressure stripping, strangulation, and harassment (Hirschmann et al. 2014b; Peng et al. 2015; Book & Benson 2010; Boselli et al. 2016; Smethurst et al. 2017). As such, environmentally-driven processes might play a direct role in affecting the galaxies' cold gas reservoir. Stellar and AGN feedback can also contribute to ejecting gas out of the galaxies. On the one hand, when the most massive stars explode as supernovae, the energy released can initiate galactic fountains (Chevalier & Clegg 1985). On the other hand, during episodes of high accretion, the SMBH has enough energy to eject cold gas from the galaxy through momentum-driven winds (Di Matteo et al. 2005; Ishibashi & Fabian 2012). These winds can result from the radiation pressure of the AGN as well as energy shocks from the accretion disk (Faucher-Giguère & Quataert 2012; Thompson et al. 2015; Ishibashi & Fabian 2015; Costa et al. 2018). As such, stellar and AGN feedback-driven winds can expel enough gas from the galaxy, which limits star formation.

In this way, the causes of quenching can range from external to internal processes which influence the gas reservoir in a galaxy and thus suppress star formation. Whether cold gas does not enter the galaxy, or the gas is heated, consumed, and removed at a faster rate than it can cool, stellar feedback plays a subordinate role to quenching. While environmental effects are thought to be the main quenching channel for low mass galaxies ( $M_{\text{stellar}}$  below  $\approx 10^{10} M_{\odot}$ , Peng et al. 2015), AGN are likely key to the long-term quiescence of massive systems. For example, in low redshift observed galaxies, Terrazas et al. (2017) show that star formation rate is a decreasing function of SMBH mass, establishing AGN as important to regulating the star formation in the local Universe. At low redshifts, high-energy outflows from AGN can contribute to star formation quenching through expelling gas from the central regions of massive galaxies, as detected by ionized winds and outflows of molecular gas in galaxies with AGN (Feruglio et al. 2010; Fischer et al. 2010; Sturm et al. 2011; Westmoquette et al. 2012; Rupke & Veilleux 2013; Harrison et al. 2014). There is also observational evidence for AGN feedback at high redshifts, where nebular emission is found in broadline quasars (Arav et al. 2013; Cano-Díaz et al. 2012; Cicone et al. 2014; Genzel et al. 2014; Förster Schreiber et al. 2014; Harrison et al. 2015). In principle, the energy output from quasars should be able to deplete the gas reservoir of galaxies (King & Pounds 2015). However, it can be difficult to draw a causal connection between AGN feedback and quiescence, since AGN feedback is so rare and highly variable, particularly in high-redshift observations. Moreover, AGN activity in such observations is often coupled with recent mergers, making it challenging to isolate the exact impact of SMBH feedback (Schreiber et al. 2019).

For determining whether AGN feedback is indeed responsible for suppressing star-formation in galaxies, theoretical models and simulations are a valuable informative tool. Semi-analytical models (combined with  $N$ -body simulations or extended Press-Schechter

based merger trees) initially suggested the ability of AGN feedback to create and maintain quenched massive galaxies, given the amount of energy released by growing SMBHs (Croton et al. 2006; Bower et al. 2006; Somerville et al. 2008). Using subgrid models for AGN feedback, numerical simulations also confirm that this process is not only able, but is also required, to regulate star formation in massive halos and reproduce the observed co-evolution between SMBH and galaxy masses (Di Matteo et al. 2005; Springel et al. 2005; Sijacki et al. 2007; Dubois et al. 2012; Choi et al. 2015). AGN feedback is hence one of the key ingredients to reproducing the massive end of the galaxy stellar mass function, and is needed to emulate quenched fractions of massive galaxies that agree with low-redshift observations in cosmological simulations. These include Magneticum (Hirschmann et al. 2014a; Bocquet et al. 2016), Illustris (Vogelsberger et al. 2014), EAGLE (Schaye et al. 2015), Horizon-AGN (Dubois et al. 2016), IllustrisTNG (Springel et al. 2018; Pillepich et al. 2018; Naiman et al. 2018; Nelson et al. 2018; Marinacci et al. 2018; Nelson et al. 2019) and Simba (Davé et al. 2019).

From the perspective of observations at  $z = 3 - 4$ , Schreiber et al. (2018); Merlin et al. (2019); Girelli et al. (2019); Cecchi et al. (2019); Valentino et al. (2020); Santini et al. (2021) all demonstrate the overall, qualitative agreement of quiescent<sup>2</sup> massive galaxies with theoretical predictions from most current hydrodynamic simulations, however with an increasing tension at higher redshifts. Recently, a growing number of massive quenched galaxies have been observed at  $z \geq 3$  (Forrest et al. 2020; Gould et al. 2023; Antwi-Danso et al. 2023b), especially with the James Webb Space Telescope (JWST, Nanayakkara et al. 2022; Carnall et al. 2023a,b; Long et al. 2023; Valentino et al. 2023), further confirming the difficulty for cosmological simulations to recover the expected number density of massive quenched galaxies at increasing redshifts. This poses a challenge to our current understanding of star formation activity in galaxy evolution, which struggles to capture the rapid growth and sudden halt of the stellar mass assembly of galaxies as massive as  $M_{\text{stellar}} = 10^{10} - 10^{11} M_{\odot}$  less than  $\sim 2$  Gyr after the Big Bang.

Because of previously limited and scarce observational data, there are only a few theoretical works which study the causes of quenching in massive galaxies beyond the local Universe (Hartley et al. 2023; Lovell et al. 2023; Lagos et al. 2023). Studies that focus on  $z \leq 2$  show that simulated quiescent and massive galaxies are strongly influenced by AGN-driven energy injections (Donnari et al. 2021a; Park et al. 2022, 2023). While there are hints that AGN feedback already contributes to halting star formation in the early Universe (e.g. Hartley et al. 2023 who focus on five massive quenched galaxies in the IllustrisTNG simulation, or Lovell et al. 2023 in the FLARES simulations at  $z \leq 5$ ), it remains to be determined if galaxy mergers, which occur frequently at high-redshift, and the large-scale environment, by affecting the fueling of gas from filaments onto a halo, play any role in quenching massive galaxies at early cosmic times. Therefore, disentangling whether AGN feedback, merger events, and large-scale structure are responsible for the quenching of massive galaxies at  $z > 3$  is the purpose of this study.

In this paper, we investigate the processes that lead to the suppression of star formation in high-redshift, massive galaxies using the cosmological simulation suite IllustrisTNG. Our method for selecting and analyzing galaxies of interest is described in § 2. Then, § 3 looks at the effect of AGN feedback, merger events, and large-scale structure in causing quiescence. Next, § 4 discusses the importance

<sup>1</sup> In some observations, jets can also occur in radiatively efficient AGN as exceptions (Hardcastle 2018; Hardcastle & Croston 2020).

<sup>2</sup> In this work, we do not make any distinction between quiescent and quenched galaxies, and we use both words interchangeably.

of the different quenching mechanisms in this study and in other cosmological simulations, and states the limitations which may explain why simulations are in tension with the observed number densities of massive quiescent galaxies at  $z \geq 3$ . We conclude in § 5 that AGN feedback is the most likely origin of quiescent massive galaxies at high redshifts in IllustrisTNG, with environmental conditions as an underlying contributing factor.

## 2 METHODOLOGY

In this section, we describe the simulations, feedback models, and selection procedure of the paper.

### 2.1 IllustrisTNG simulations

We investigate the cause of quenching in high-redshift, massive galaxies using the cosmological simulation suite, IllustrisTNG (TNG; Nelson et al. 2019). These simulations are performed with the AREPO code (Springel 2010), which solves the equations of magnetohydrodynamics and self-gravity using a moving-mesh technique. The TNG simulations include various physical processes such as gas cooling, star formation, stellar feedback and AGN feedback, as described in detail by Weinberger et al. (2017) and Pillepich et al. (2017).

We utilize the highest resolution realizations of the TNG100 and TNG300 simulations (TNG100-1 and TNG300-1 from Springel et al. 2018; Pillepich et al. 2018; Naiman et al. 2018; Nelson et al. 2018; Marinacci et al. 2018), which consist of large cosmological boxes of volume  $110^3 \text{ cMpc}^3$  and  $302^3 \text{ cMpc}^3$ , respectively. More specifically, TNG100 has  $1820^3$  initial dark matter particles with a mass resolution of  $7.5 \times 10^6 M_\odot$ , and has a baryonic mass resolution of  $1.6 \times 10^6 M_\odot$ . The mass resolution in TNG300 is lower, and reaches  $5.9 \times 10^7 M_\odot$  for dark matter particles and  $1.1 \times 10^7 M_\odot$  for baryons. We use both simulations because, while TNG100 provides better resolution, TNG300 allows for the formation of more numerous and more massive galaxies due to its larger volume.

### 2.2 Star formation and stellar feedback

The way in which galaxies become quiescent depends on *how* stars are able to form in the simulation. Due to resolution limits, TNG treats star formation in a subgrid framework and relies on the pressurization of a multi-phase ISM model. Stars stochastically form from gas cells that reach above the density threshold  $n_H = 0.1 \text{ cm}^{-3}$ , with pressurization from unresolved supernovae included in the star-forming gas. As a consequence of this star formation model, galaxies in the TNG simulations quench when there is not enough dense gas. Taking into account additional criteria such as gas temperature, velocity dispersion, or turbulence, would change the star formation history and the quiescent state of the galaxies, but such a study is beyond the scope of this paper. Feedback from star formation is assumed to drive galactic-scale outflows in the form of winds. However, we do not go into detail on the implementation of stellar feedback since it has been shown to be ineffective toward quenching massive galaxies in the literature.

### 2.3 SMBH activity and AGN feedback

Because we are especially interested in the role of central SMBHs in suppressing star formation in massive high-redshift galaxies, we briefly summarize how black holes are seeded, how they grow, and

how AGN feedback acts in the TNG simulations. More details can be found in the reference papers from Vogelsberger et al. (2013) and Weinberger et al. (2017).

The TNG model places a black hole with seed mass of  $M_{\text{seed}} = 8 \times 10^5 h^{-1} M_\odot$  in a friends-of-friends (FoF) halo when it exceeds  $M_{\text{FoF}} = 5 \times 10^{10} h^{-1} M_\odot$ . Here, FoF halo refers to a gravitationally bound dark matter halo as determined by the SUBFIND algorithm (Springel et al. 2001). Haloes are then tracked in time using merger trees that are obtained using the SubLink algorithm from Rodriguez-Gomez et al. (2015). This algorithm identifies unique descendants and chooses the main progenitors of each galaxy with the “most massive history” behind it.

Once a black hole is seeded, it grows at a rate which follows the Bondi-Hoyle-Lyttleton accretion rate  $\dot{M}_{\text{Bondi}}$ , limited to the Eddington rate  $\dot{M}_{\text{Edd}}$ . Additionally, a black hole may grow by merging with another one during a galaxy merger event. As a consequence from black hole accretion, energy is released to the surrounding gas cells, which we refer to as AGN feedback. Whether the energy is released as thermal or kinetic energy depends on the Eddington ratio  $f_{\text{Edd}} = \dot{M}_{\text{Bondi}}/\dot{M}_{\text{Edd}}$ . This value describes how strongly a black hole is accreting relative to its maximum possible accretion rate and is dependent upon the mass of the black hole squared. In TNG, the Eddington ratio is compared to a threshold called “ $\chi$ ”: whenever the Eddington ratio is above this threshold and the accretion rate is high, AGN feedback operates via the deposit of thermal energy  $E_{\text{inj, therm}}$  in the quasar mode. Conversely, when  $f_{\text{Edd}} < \chi$ , the energy  $E_{\text{inj, kin}}$  is imparted as random kinetic kicks in the so-called kinetic, radiatively inefficient jet mode feedback. The original TNG methods paper for black hole feedback Weinberger et al. (2017) gives detailed definitions of the above quantities, but we also provide them here for completeness:

$$\dot{M}_{\text{Bondi}} = \frac{4\pi G^2 M_{\text{BH}}^2 \rho}{c_s^3}, \quad (1)$$

$$\dot{M}_{\text{Edd}} = \frac{4\pi G^2 M_{\text{BH}} m_p \rho}{\epsilon_r \sigma_T c}, \quad (2)$$

$$\chi = \min \left[ \chi_0 \times \left( \frac{M_{\text{BH}}}{10^8 M_\odot} \right)^\beta, 0.1 \right]. \quad (3)$$

In Equations 1 and 2,  $G$  is the universal gravitational constant,  $m_p$  the proton mass,  $\epsilon_r$  the radiative accretion efficiency,  $\sigma_T$  the Thompson cross-section, and  $c$  the vacuum speed of light.  $M_{\text{BH}}$  is the black hole mass, and  $\rho$  and  $c_s$  are the density and sound speed of the gas near the black hole, respectively. In Equation 3,  $\chi_0 = 0.002$  and  $\beta = 2$  which are the fiducial values adopted in TNG. The functional form of  $\chi$  is such that even the most massive black holes in the simulation can reach the quasar feedback mode, while it would be difficult for low mass black holes to reach the jet feedback mode. This heuristic formulation of  $\chi$  is meant to support the quenching of massive galaxies. In the raw TNG data outputs, the quasar-mode and jet mode feedback of the AGN are moreover given as cumulative energy injections over time. We estimate the time-averaged energy injection rate, or power  $\dot{E}_{\text{inj, therm}}$  or  $\dot{E}_{\text{inj, kin}}$ , as the change in  $E_{\text{inj, therm}}$  or  $E_{\text{inj, kin}}$ , divided by the difference in cosmic time between snapshots.

It should be highlighted that the AGN feedback mechanisms are not themselves resolved, and in general, cannot be resolved in cosmological simulations which rely on subgrid models (for example, Schaye et al. 2015 in EAGLE and Henden et al. 2018 in FABLE too). Rather, the TNG works to capture the large-scale impact of the quasar and jets through their effect on the gas cells around the black hole. For example, TNG constructs the jet mode to efficiently reg-

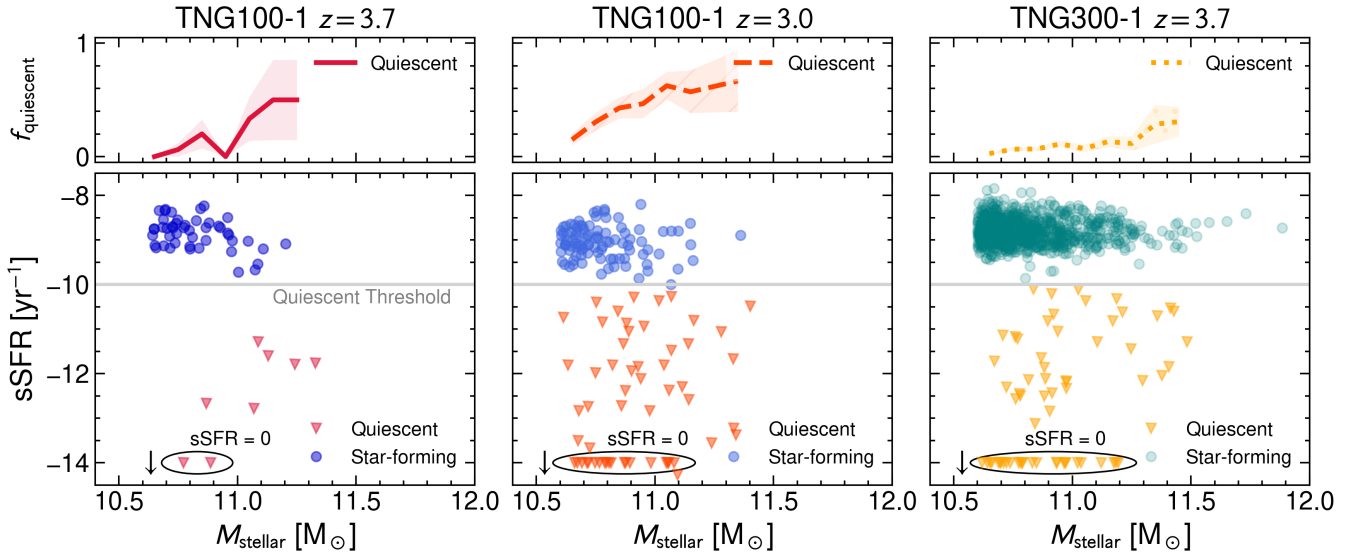


**Figure 1. Quiescent and Star-forming Samples.** Fraction of quiescent galaxies (top row) and specific star formation rate (bottom row) versus stellar mass for the TNG100-1  $z = 3.7$  (left), TNG100-1  $z = 3.0$  (middle), and TNG300-1  $z = 3.7$  (right) samples. In each panel, we compare the quiescent (red shade, triangles) and star-forming (blue shade, circles) galaxies. We select galaxies above a mass-cut  $M_{\text{stellar}} \geq 10^{10.6} M_{\odot}$ . Then, we define quiescent galaxies as having specific star formation rates in the range  $\text{sSFR} \leq 10^{-10} \text{ yr}^{-1}$ . The star-forming galaxies in our selection have sSFR values above this threshold (gray, solid line). Some galaxies in the quiescent samples have  $\text{sSFR} = 0 \text{ yr}^{-1}$ , as they have zero star-forming gas cells; these objects are circled in black and indicated with a downward arrow. In each simulation sample, there are more star-forming than quiescent galaxies, and the fraction of quiescent galaxies increases with stellar mass.

Simulation	Redshift	# Quiescent	# Star-forming
1. TNG100-1	$z = 3.7$	8	47
2. TNG100-1	$z = 3.0$	56	99
3. TNG300-1	$z = 3.7$	65	884

**Table 1. Selected Galaxies in TNG.** We use three different samples in this work, and include their respective numbers of quiescent and star-forming galaxies here.

ulate the growth of massive galaxies. This feature of cosmological simulations leads to parameterizations which are somewhat numerically rather than entirely physically motivated, in order to reproduce realistic galaxy populations in the the local Universe. As a preliminary note, other simulations use different subgrid feedback models to obtain similar low-redshift galaxy populations: following the examples above, EAGLE makes use of a single efficient thermal mode, and FABLE has a stronger quasar mode than that of TNG together with the jet mode used in the Illustris simulations (Genel et al. 2014; Vogelsberger et al. 2014; Sijacki et al. 2015). The choice of modeling will inherently impact our interpretation of what quenches massive high- $z$  galaxies in these simulations, which we further examine in § 4 of the Discussion.

## 2.4 Sample selection

In order to study the high-redshift Universe, we first consider simulated galaxies at redshift  $z = 3.7$  in TNG100. We only consider resolved subhalos that have at least 1000 stellar particles and 1000 dark matter particles. Since this sample only relies on a single simulation snapshot, we also select galaxies at  $z = 3.0$  in TNG100 to assess whether or not our findings are consistent across different times in the high-redshift Universe. As a further check, we also consider the  $z = 3.7$  snapshot in TNG300 to obtain larger number statistics.

To select massive, quiescent objects, we make use of the stellar

mass and star formation content of the galaxies. We impose a mass-cut of  $M_{\text{stellar}} \geq 10^{10.6} M_{\odot}$ , as adopted by Valentino et al. (2023) to compare the number densities of quenched galaxies at  $z = 3 - 4$  in a compilation of observational works to that measured in simulations. We note that throughout the paper, we consider stellar and gas properties as the sum of all gravitationally bound star and gas particles within twice the stellar half-mass radius ( $R = 2 R_{\text{eff}}$ ) of the galaxy. Then, we define quiescent galaxies as having specific star formation rates, or the ratio between star formation rate and stellar mass, in the range  $\text{sSFR} \leq 10^{-10} \text{ yr}^{-1}$  (following e.g. Franx et al. 2008 for  $z \approx 3.7$ ). The star-forming galaxies in our selection have sSFR values above this threshold.

This selection of galaxies based on stellar mass and star formation rates is shown in Figure 1. From left to right, we show our three samples of galaxies from TNG100 at  $z = 3.7$ , at  $z = 3.0$ , and from TNG300 at  $z = 3.7$ . Quenched galaxies are represented with red symbols, while star-forming galaxies are shown by blue symbols. We adopt the same coloring scheme for all plots throughout the paper. The top panels of Figure 1 show that the fraction of quiescent galaxies ( $f_{\text{quiescent}}$ ) increases with stellar mass. In TNG100, at  $z = 3.7$ , only a few galaxies are quenched. After some time, at  $z = 3$ , lower-mass galaxies have built up: there are more galaxies with  $M_{\text{stellar}} \geq 10^{10.6} M_{\odot}$ , and more of them are quenched at this redshift than at  $z = 3.7$ . TNG300 provides the larger sample for both quenched and star-forming massive galaxies. At the high-mass end, only a handful of galaxies are quiescent so that  $f_{\text{quiescent}}$  is smaller for this sample than for those from TNG100 (in the latter, there are only two galaxies, which is not statistically significant). The quiescent fractions are overall lower in TNG300 than in the TNG100 samples, probably due to resolution limits, and the fact that the stellar mass of halos of a given total mass is slightly lower in TNG300 compared to TNG100 (Pillepich et al. 2018; Vogelsberger et al. 2018). This implies that there is less feedback at the internal and environmental scales in the larger simulation box when considering stellar mass bins. To better

appreciate the distribution of quiescent and star-forming galaxies, the bottom panel of Figure 1 shows the specific star formation rate as a function of stellar mass. The grey horizontal line represents our quiescent threshold of  $sSFR = 10^{-10} \text{ yr}^{-1}$ . Overall, the number of quiescent galaxies is lower than their star-forming counterparts in our samples. To summarize, the three different simulation samples consist of massive galaxies from Table 1. Throughout this study, we will present the findings for each of these three samples.

### 3 RESULTS

We consider three possible causes of quenching at high redshifts in massive galaxies: internal SMBH feedback, mergers with other galaxies, and the indirect influence of the large-scale environment. Later in the discussion, § 4, we explore the impact of these quenching mechanisms on the gas reservoirs of the galaxies.

#### 3.1 Influence of AGN feedback

First, we want to determine if feedback from the central SMBH is an important cause of quiescence at high redshifts.

##### 3.1.1 SMBH mass growth

As we mentioned in § 2.3, in TNG, a black hole is seeded in a galaxy once its host halo mass exceeds a certain mass,  $M_{\text{FoF}} = 5 \times 10^{10} h^{-1} M_{\odot}$ . The time at which this occurs in a galaxy is called the ‘‘BH seed time,’’ and gives information as to when the central SMBH starts growing and releasing energy into the ISM.

In order to have a better understanding of SMBH growth in our galaxies, which may vary depending on the gas supply available, we introduce the ‘‘critical time of SMBH mass growth.’’ We arbitrarily define this as the time at which a SMBH first exceeds  $M_{\text{BH}} \geq 10^{6.5} M_{\odot}$  in mass. This happens relatively soon after the black hole seeds and roughly corresponds to when the black hole has doubled its initial mass, which is  $M_{\text{BH}} = 8 \times 10^5 h^{-1} M_{\odot} \approx 1.2 \times 10^6 M_{\odot}$ . This definition provides a more stable criterion for detecting the seeding of black holes in the simulation.

Following the above definition, Figure 2 shows histograms of the redshift corresponding to the critical time of SMBH mass growth, for both the quiescent (red shades) and star-forming (blue shades) samples across our three simulation sets. The thick lines show the distribution of redshift, and the thin vertical lines correspond to the average redshift, with the  $1-\sigma$  standard deviation to the mean shown with a translucent area. The SMBHs of the quiescent galaxies seed earlier and reach  $M_{\text{BH}} \geq 10^{6.5} M_{\odot}$  at earlier redshifts than the star-forming galaxies. In the upper right corner of the plots, we show the  $p$ -values from the one-sided T-test for the means of the two independent galaxy samples. As they are low, this indicates that the difference in the critical time of SMBH mass growth between the star-forming and the quenched galaxies is statistically significant, especially for the TNG300 sample due to its large number statistics. Therefore, these earlier critical redshifts likely favor a faster SMBH mass growth in the quiescent samples, and consequently a longer exposure of the ISM to AGN feedback.

##### 3.1.2 Causes and consequences of SMBH growth and AGN feedback

The consequences from SMBH growth and feedback taking effect earlier in the quiescent galaxies are shown in detail in Figure 3. This

figure shows the mean-averaged time evolution of stellar, dark matter, and SMBH properties of the simulated galaxies. From the top row to the bottom row, we respectively focus on the specific star formation rate, stellar mass, dark matter mass, dark matter accretion rate<sup>3</sup>, SMBH mass, Eddington ratio, AGN thermal energy injection rate, AGN kinetic energy injection rate, and ratio between the Eddington ratio and  $\chi$  (defined in § 2.3). We note that dark matter properties are calculated from all particles of this type within the subhalo. We additionally indicate the time at which our samples of galaxies are selected with grey vertical lines, as well as the period between the critical time of SMBH mass growth, the onset of the AGN jet mode, and the time of quiescence<sup>4</sup> with respective markers.

On average, the specific star formation rates of the quiescent and star-forming galaxies are comparable until they diverge just before  $z = 4.0$ , which is approximately when we select our samples. At this point, the sSFRs of the quiescent samples experience a sharp drop below that of the star-forming samples. The purpose of this subsection is to investigate if this sudden decrease in star formation is related to AGN feedback.

Continuing with Figure 3, we see that the average stellar mass of the quiescent galaxies is consistently higher than that of the star-forming galaxies since the beginning of their evolution. This would suggest higher SMBH masses according to known scaling relations (Kormendy & Ho 2013), in line with the trend we actually measure. We also highlight that quiescent galaxies are overall hosted in more massive halos by  $\sim 0.4$ dex, and consequently have higher dark matter mass accretion rates, particularly for the TNG100  $z = 3.7$  and  $z = 3.0$  samples.

As a consequence from their stronger gravitational attraction (and because they reside in high-density peaks, see also § 3.3), the quiescent galaxies also initially have more gas supply, which favours star formation and SMBH growth. The halos hosting the quiescent galaxies become massive enough to host a SMBH earlier than their star-forming counterparts (when  $M_{\text{FoF}} > 5 \times 10^{10} h^{-1} M_{\odot}$ ), as already shown with the critical time of SMBH mass growth in Figure 2. Indeed, when we check narrower halo mass and stellar mass bins, the time difference between when black holes seed in the quiescent and star-forming samples becomes less significant. Having their black hole sink particle seeded earlier is another explanation for the faster SMBH growth for the quiescent galaxies, which we further illustrate via the Eddington ratio: the SMBH accretion rate experiences a higher peak in the quiescent galaxies just before their SMBHs reach our defined critical mass of  $M_{\text{BH}} \geq 10^{6.5} M_{\odot}$ , and until their sSFRs begin to decrease. When the galaxies become quiescent, the Eddington ratio decreases and the SMBH mass almost stops growing.

In order to better study the interplay between AGN feedback and star formation, we now focus on the energy released by the SMBHs as a consequence from their accretion. As discussed in § 3.1, in TNG, this energy is released either as thermal or kinetic energy if the Eddington ratio is higher or lower than a value  $\chi$  (defined in § 2.3), respectively.

From the last three bottom rows of Figure 3, we see that at early stages, from the time that the black hole seeds up to the time of quiescence, AGN feedback mainly consists in thermal energy injections. To remind the reader, we calculate the time-averaged energy injected

<sup>3</sup> We calculate  $\dot{M}_{\text{DM}}$  using the net change of the dark matter mass over the time-difference between simulation snapshots.

<sup>4</sup> The time of quiescence for the star-forming samples corresponds to an average value which does not include galaxies with  $M_{\text{stellar}} < 10^{10.6} M_{\odot}$  that will reach this stellar mass later, after our selection time.

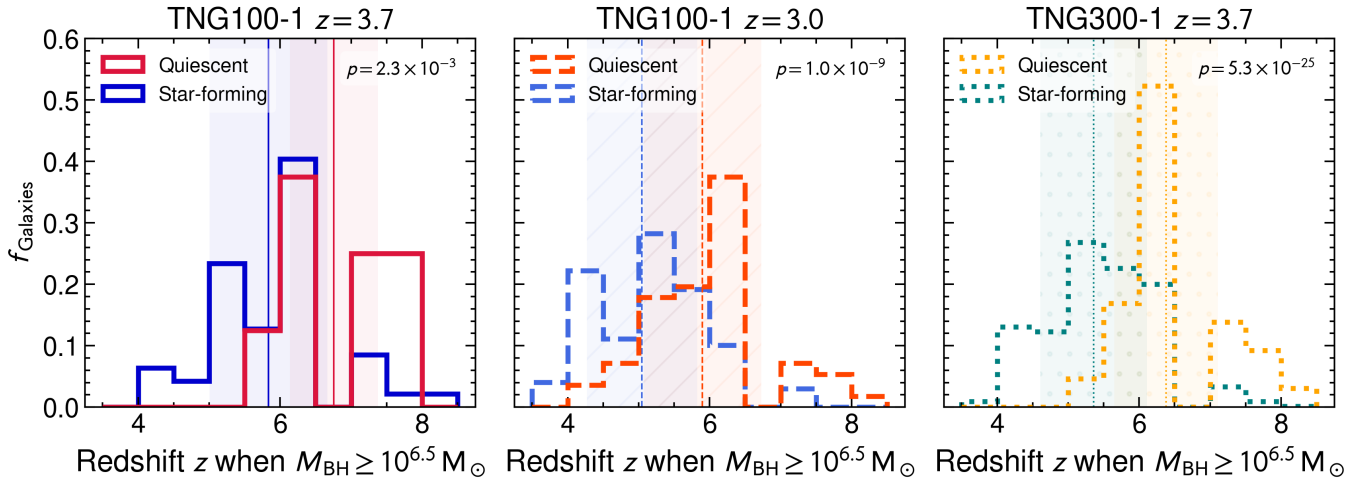


**Figure 2. Impact of Black Hole Seeding.** Relative frequency of galaxies with respect to the critical time of SMBH mass growth. We define the “critical time of SMBH mass growth” as the time when the galaxy’s central black hole mass exceeds  $M_{\text{BH}} \geq 10^{6.5} M_{\odot}$ . We show separate histograms for the TNG100-1  $z = 3.7$  (left, solid), TNG100-1  $z = 3.0$  (middle, dashed), and TNG300-1  $z = 3.7$  (right, dotted) samples. We also compare the histograms of the quiescent (red shades) and star-forming (blue shades) galaxies in each panel, by indicating their mean-averages (vertical lines) and standard-deviations (translucent areas). In each simulation sample, the quiescent galaxies reach the critical SMBH mass at significantly earlier times than the star-forming galaxies (as also confirmed by the low  $p$ -values from the one-sided T-test of the means, shown in the upper right corners).

by dividing the change in energy by the difference in cosmic time between snapshots. SMBHs hosted in the quiescent galaxies are overall more massive than those hosted in galaxies from our star-forming samples, and as a result they contribute to more thermal energy injections. This is because the total energy injected is by definition proportional to the SMBH accretion rate, and hence scales with the SMBH mass squared. The turnover time at which the AGN goes from a thermal, quasar mode to a kinetic, jet mode is also a function of SMBH mass squared (via  $\chi$ ), and therefore SMBHs from the quiescent galaxy samples fall in the kinetic feedback regime earlier than star-forming galaxies.

Thus, on average, the quiescent galaxies in the TNG simulations experience a greater injection of kinetic energy, which has been shown to be the most efficient feedback channel to affect massive galaxies and their star formation at low redshifts (e.g. Terrazas et al. 2020). We also note that in our three simulation sets, the time at which the kinetic jet mode of AGN feedback is triggered coincides with the time of quiescence. From this population-based analysis, it is not immediately clear whether the galaxies become quenched first and the jet mode simply maintains their quiescence, or vice versa. Zoom-in simulations of individual galaxies are required, and initial explorations indicate that the AGN jets are indeed driving the quenching process (Farcy et al. in preparation). Nevertheless, it is apparent that SMBH activity is likely connected to the drop in star formation of these massive galaxies.

From this first analysis, we conclude that in addition to having earlier black hole seed times on average, the greater SMBH activity in the quiescent galaxies must be driven by progenitor bias from higher initial halo masses. At a given time, the SMBHs from our samples of quenched galaxies are more massive, have a stronger accretion activity, and inject more energy to the surrounding gas. Once the SMBHs are massive enough and at the same time have an accretion rate small enough, they trigger the kinetic, radiatively inefficient AGN feedback mode, which coincides with a drop in sSFR and with the time of quiescence.

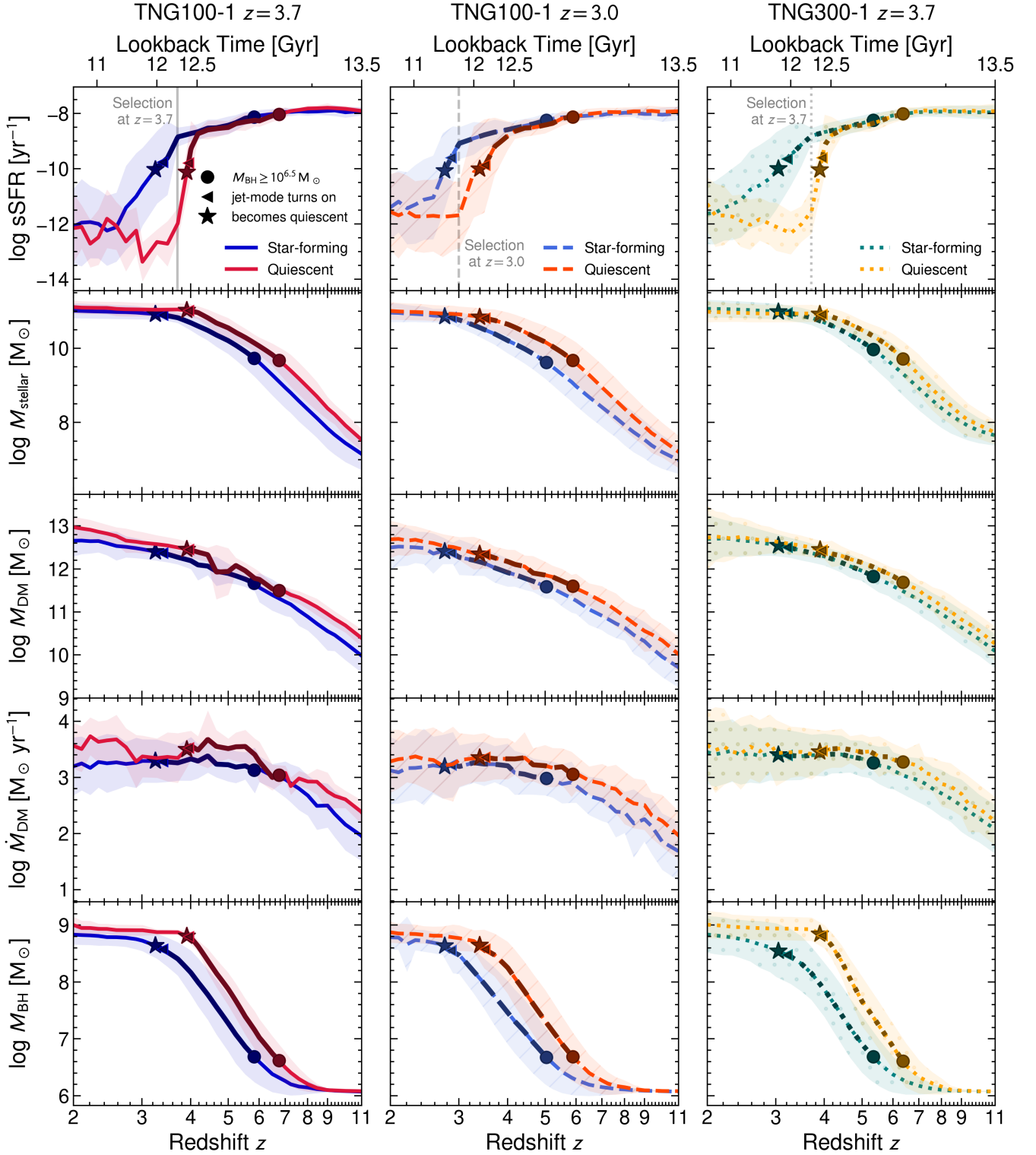
### 3.2 Negligible role of merger events

We just showed that SMBH feedback plays an important role in quenching massive galaxies earlier in their lifetimes. Now, we focus on the potential effect of merger events.

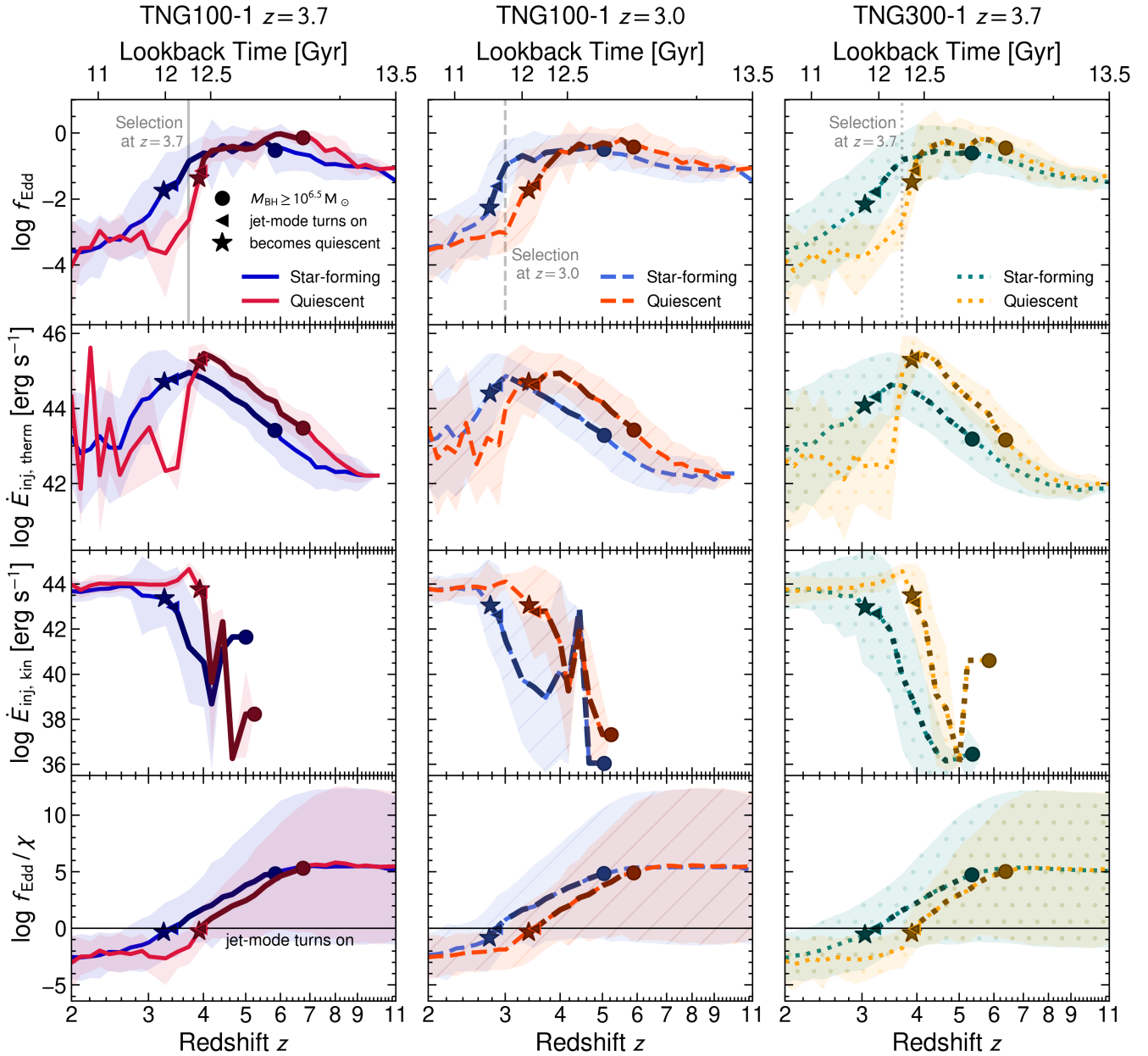
The internal properties of a galaxy can be directly impacted by close encounters and interactions with nearby subhalos. We investigate the effect of minor and major merger events on internal galactic properties through tracing the main branch of the galaxies’ merger trees back in time. This allows us to determine if quiescent and star-forming galaxies experience different merger histories, and, accordingly, if their stellar, gas, and SMBH evolutions may be related. In our analysis, we define “minor” mergers as merger events between galaxies with a mass ratio between 1:10 and 1:4. We identify “major” merger events as having a minimum mass ratio of 1:4. In other words, we consider that a given galaxy has experienced a major (minor) merger if it became the main progenitor of a galaxy that was up to 4 times (between 4 and 10 times) less massive.

Figure 4 shows the fraction of quiescent and star-forming galaxies that experience each type of merger as a function of redshift (first two rows), and as a function of the total number of mergers at the redshift when galaxy samples are selected (last two rows).

Focusing first on the redshift evolution, we see that the overall distribution of major and minor merger events is not significantly different between the quiescent and star-forming galaxies. Although the quiescent galaxies in the TNG100  $z = 3.7$  sample experience a higher peak in the minor merger events at  $z \approx 10$ , this feature does not appear in the TNG100  $z = 3.0$  and TNG300  $z = 3.7$  simulation sets. The mean fraction of both minor and major mergers, shown with thin horizontal lines, is very similar for both populations of galaxies, revealing that they have very similar merger histories. In addition, the two bottom rows of Figure 4 show that the quiescent galaxies do not experience significantly more minor or major mergers than the star-forming galaxies. This is further confirmed by the fact that the  $p$ -values approach unity, as shown in the top right corner of the plots. If we look at the average number of merger events, shown with thin vertical lines, most quiescent and star-forming galaxies have ex-



**Figure 3. Stellar, Dark Matter, and SMBH Histories.** Redshift evolution between  $z = 2$  to 11 of various galactic properties for the TNG100-1  $z = 3.7$  (left, solid), TNG100-1  $z = 3.0$  (middle, dashed), and TNG300-1  $z = 3.7$  (right, dotted) samples. In each panel, we compare the quiescent (red shades) and star-forming (blue shades) galaxies, by indicating their mean-averaged values and standard-deviations (translucent regions). We also indicate the average period (bolded segments) between when the galaxies' SMBH masses first exceeded  $10^{6.5} M_{\odot}$  (circle), when their AGN switched to the jet mode (triangle), and the time of quiescence (star). From top to bottom, we show the logarithms of specific star formation rate (sSFR), stellar mass ( $M_{\text{stellar}}$ ), halo dark matter mass ( $M_{\text{DM}}$ ), dark matter accretion rate ( $\dot{M}_{\text{DM}}$ ), and SMBH mass ( $M_{\text{BH}}$ ). In general, the sSFR (first row) of quiescent galaxies decreases below that of the star-forming galaxies before  $z = 4.0$ . Before they begin quenching, the quiescent galaxies also experience earlier and faster stellar mass growth (second row). Because they are hosted in more massive halos (third row), the quiescent galaxies experience higher dark matter mass accretion rates (fourth row). Together, the stellar and dark matter mass growth likely drive the accelerated mass growth of the galaxies' central SMBHs (fifth row).



**Figure 3. (continued)** Redshift evolutions of Eddington ratio  $f_{\text{Edd}}$ , AGN thermal energy injection rate ( $\dot{E}_{\text{inj, therm}}$ ), AGN kinetic energy injection rate ( $\dot{E}_{\text{inj, kin}}$ ), and ratio between the Eddington ratio and the threshold for thermal to kinetic energy injection  $\chi$ . The horizontal line in the bottom panels show the limit above (below) which thermal (kinetic) energy is injected from the AGN. While  $\log f_{\text{Edd}}/\chi > 0$ , most of the energy injected by the SMBH is in the thermal form (by definition). Before the time of quenching, SMBHs in the quiescent galaxies have higher accretion rates, thus a higher Eddington factor, and inject more energy in the thermal form. Then, the kinetic jet mode of AGN feedback is triggered—which happens slightly before, if not at, the time of quiescence—and from this point, kinetic energy injections dominate the AGN feedback energy budget. All of these results appear to be consistent between each simulation sample.

perienced less than three minor mergers, and only around one major merger, by the time we “observe” them in the specified snapshots. Overall, this shows that there is no excess of recent major nor minor mergers in the quiescent galaxies. Therefore, the IllustrisTNG simulations do not predict that the quiescence of high-redshift massive galaxies is related to any merger-driven starbursts that would have depleted the galaxies from most of their star-forming, cold gas reservoirs (Man & Belli 2018).

### 3.3 Large-scale environment

In § 3.1, we explored the impact of SMBH growth and AGN feedback on star formation quenching in high-redshift massive galaxies, and in § 3.2, we also assessed whether mergers are an external cause of quenching. In this section, we will investigate the influence of the large-scale environment: that is, if the location of galaxies within the cosmic web may favour their quiescence.

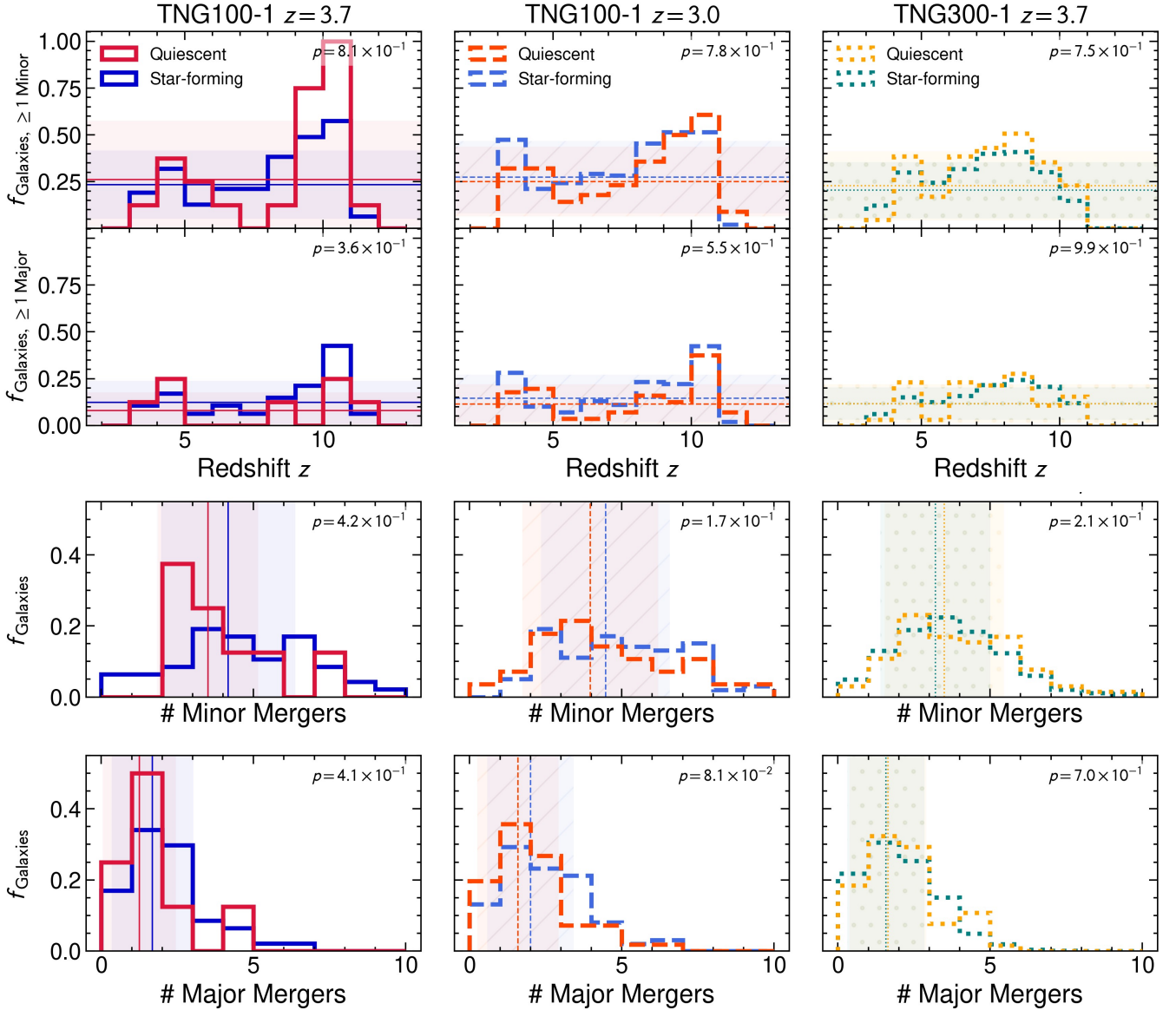


**Figure 4. Impact of Minor and Major Mergers.** Histograms of the fraction of galaxies that experience merger events in the TNG100-1  $z = 3.7$  (left, solid), TNG100-1  $z = 3.0$  (middle, dashed), and TNG300-1  $z = 3.7$  (right, dotted) samples. We also compare the histograms of the quiescent (red shades) and star-forming (blue shades) galaxies in each panel, by indicating their mean-averages (horizontal and vertical lines) and standard-deviations (translucent boxes). *First and second rows:* fraction of galaxies with respect to redshift that experience at least one minor or major merger with minimum mass ratios of  $> 1 : 10$  and  $> 1 : 4$ , respectively. For each simulation sample, the distribution of mergers over time is similar between the quiescent and star-forming galaxies. *Third and fourth rows:* fraction of galaxies with respect to the number of past minor and major merger events. The quiescent galaxies do not experience significantly more mergers than the star-forming galaxies (as also confirmed by the  $p$ -values approaching unity, shown in the upper right corners). In this way, mergers between galaxies are likely unimportant to the quenching of these galaxies at high-redshift.

### 3.3.1 Residence time in a massive host halo

One way to characterize the environment of the galaxies is through looking at the dark matter content of their host halos, namely the mass  $M_{\text{host}}$ . In particular, one of the conclusions from Figure 3 is that quenched galaxies are globally hosted in halos more massive than star-forming galaxies.

To complement this result, we determine if the quenched galaxies have different large-scale environmental conditions through time compared to star-forming galaxies by computing the amount of time they spend in host halos more massive than  $M_{\text{host}} \geq 10^{12} M_{\odot}$ . When-

ever the subhalo is a satellite galaxy,<sup>5</sup> we will consider the dark matter mass of its host halo. Figure 5 shows histograms of the relative frequency of quiescent and star-forming galaxies with respect to the total amount of time they have been in massive host halos, for all simulation sets. On average, the quiescent galaxies spend statistically more time in a massive host halo than star-forming galaxies, as indicated by the very small  $p$ -values. However, the right tail of the

<sup>5</sup> Only a small percentage of our selected galaxies are satellites, whereas the vast majority are centrals as expected from a hierarchical structure formation scenario.

blue histograms shows that there is a sub-population of star-forming galaxies which spend a similarly large amount of time in a massive host halo. Thus, a dense environment could be a necessary, but not sufficient, condition for quiescence at high-redshift.

### 3.3.2 Number of neighboring satellite galaxies

The host halo mass provides a general sense of the environment that a galaxy is in. As an additional check, we also measure the environmental “over”-density through counting the number of neighboring satellites within 1 cMpc of each galaxy of interest. As stated in § 2.4, we only consider resolved subhalos that have at least 1000 stellar particles ( $M_{\text{stellar}} \geq 1.4 \times 10^9 M_{\odot}$  for TNG100 and  $\geq 1.1 \times 10^{10} M_{\odot}$  for TNG300) and 1000 dark matter particles ( $M_{\text{DM}} \geq 7.5 \times 10^9 M_{\odot}$  in TNG100 and  $\geq 5.9 \times 10^{10} M_{\odot}$  in TNG300). Figure 6 shows the time evolution of the average number of neighbours within a 1 cMpc sphere centered around the quiescent and star-forming objects, in the same style as Figure 3. Overall, the quiescent galaxies reside in slightly more dense regions, especially before and after the SMBH mass growth-to-quenching period. Because we only count the number of galaxies well resolved in terms of dark matter and stellar content, we identify only a few neighbours around each target halo, and their number increases with decreasing redshift as more subhalos reach the dark matter and stellar mass cuts.

Together with Figure 5, Figure 6 shows that quiescent massive galaxies sit in higher density peaks compared to star-forming galaxies. Therefore, quenched galaxies from our samples are able to evolve faster as they have more gas accretion along filaments, leading to faster galaxy and SMBH growth (as shown in Figure 3). Because SMBH growth is related to AGN feedback, this may be responsible for shutting down star formation in the end.

## 4 DISCUSSION

In the previous section, we put emphasis on three potential causes for quenching massive galaxies at  $z \gtrsim 3$ : SMBH growth and activity, excess of minor and major mergers, and large-scale environmental conditions. We now want to explore their consequences on the galaxies’ gas content and flows in § 4.1, compare our results with those from other studies and at different redshifts in § 4.2, and discuss the limitations of our work in § 4.3.

### 4.1 Consequences of feedback and environment

The gas content within and surrounding a galaxy can provide information about how its star-forming reservoir is influenced by internal processes like stellar and AGN feedback, versus the environment. We now want to assess the effect of the large-scale environment and of feedback on the galaxies’ gas content and flows through looking at their cold gas fraction, outflows, and inflows.

In order to characterize the amount of cold gas in a galaxy, we calculate the cold gas fraction as  $f_{\text{cold}} = M_{\text{cold gas}} / (M_{\text{cold gas}} + M_{\text{stellar}})$  following definitions by observers, where  $M_{\text{cold gas}}$  is the mass of all gas particles which have a non-zero star formation rate and a temperature  $T \leq 10^5$  K, and that belong to a sphere of twice the stellar half-mass radius ( $R = 2R_{\text{eff}}$ ). Only a small fraction of star-forming gas cells on the effective equation of state are above this temperature (for reference, see Torrey et al. 2019).

In addition, we consider the outflow and inflow rates of gas through the galaxy. To calculate the mass flow rates, we draw spherical shells centered on each galaxy, of radius  $R_{\text{galaxy}} = 7R_{\text{eff}}$  and of 1 kpc

width.<sup>6</sup> For each gas cell that belongs to this shell, the mass flow rates are then defined as the product of the gas mass with the gas radial velocity divided by the width of shell. Gas cells are considered inflowing (respectively outflowing) when they have a positive (negative) radial velocity. The total mass inflow and outflow rates are then derived by summing the values of all the cells intersected by the shells.

Figure 7 shows the time evolution of the cold gas fraction, the mass outflow rate, and the mass inflow rate (from top to bottom). Before  $z \approx 8$ , the cold gas fraction does not largely differ between the quiescent and star-forming galaxies, and before their SMBH seeds, quiescent galaxies experience greater gas mass inflow rates than the star-forming galaxies. This can be explained by the fact that quiescent galaxies are hosted in more massive halos (Figure 3) and are surrounded by a slightly denser environment (Figure 6), and therefore have more gas supply available. With time, this enables stars to form and SMBHs to grow at a faster rate in galaxies from the quiescent samples. Because of higher star formation and SMBH accretion rates, supernova feedback episodes and continuous SMBH energy injections drive more outflows in quenched than in star-forming galaxies. Both the faster gas consumption and the feedback-driven outflows lead to lower cold gas fraction for quenched galaxies throughout their lifetime.

Once the SMBHs seed, the inflow rates are not so distinguishable between the populations until the quiescent galaxies quench and their intake of cold gas decreases even more. We attribute this small drop in the mass inflow rate to the kinetic energy released by the central SMBH. In principle, the kinetic energy released in the radiatively inefficient regime has both a preventative and ejective effect: it efficiently prevents gas inflows from reaching the ISM and ejects gas far from the ISM (e.g. Ramesh et al. 2023), so that there is no fuel for star formation. While there is a small drop in the inflow rate, and even a slight decrease in the outflow rate after the time of quiescence, the cold gas fraction remains lower in quenched galaxies than in star-forming ones at any time. This shows that the gas which fuels star formation lies between the galaxies’ ISM and the outer limit we set for the subhalo ( $R_{\text{galaxy}} = 7R_{\text{eff}}$ ), where we measure the mass flow rates. Therefore, AGN feedback likely provides the pressure support for preventing gas from falling further into the galaxies, while also ejecting gas from the ISM. We note that the stellar feedback in the galaxies is negligible at this time, as there is a low number of supernova explosions when the star formation rate is so low.

To conclude this section, quenched galaxies have lower cold gas fractions and overall higher mass outflow rates, as the combined effect of gas depleted to form stars and to feed the SMBH, and of feedback-driven outflows. Mass inflow rates are higher before SMBHs seed because quenched galaxies tend to reside in more massive halos, and they are slightly suppressed when the galaxies become quenched as the result from AGN kinetic energy deposition.

### 4.2 Galaxy quenching in simulations

In this work, we find that IllustrisTNG predicts AGN feedback to be the main agent of quenching, whereas environmental conditions are

<sup>6</sup> We estimate the radius of the galaxy based on Kravtsov (2013) and Somerville et al. (2018), where the effective radius of the galaxy is found to be  $R_{\text{eff}} = 0.015R_{\text{halo}}$  in terms of the halo virial radius for massive galaxies. Assuming the entire extent of the galaxy is a tenth of the halo (Oser et al. 2010), we obtain  $R_{\text{galaxy}} \equiv R_{\text{halo}}/10 \approx 7R_{\text{eff}}$ . We also computed mass flow rates within a shell of 10 kpc in width, and with a radius of  $R_{200}$ , and the results are barely impacted.

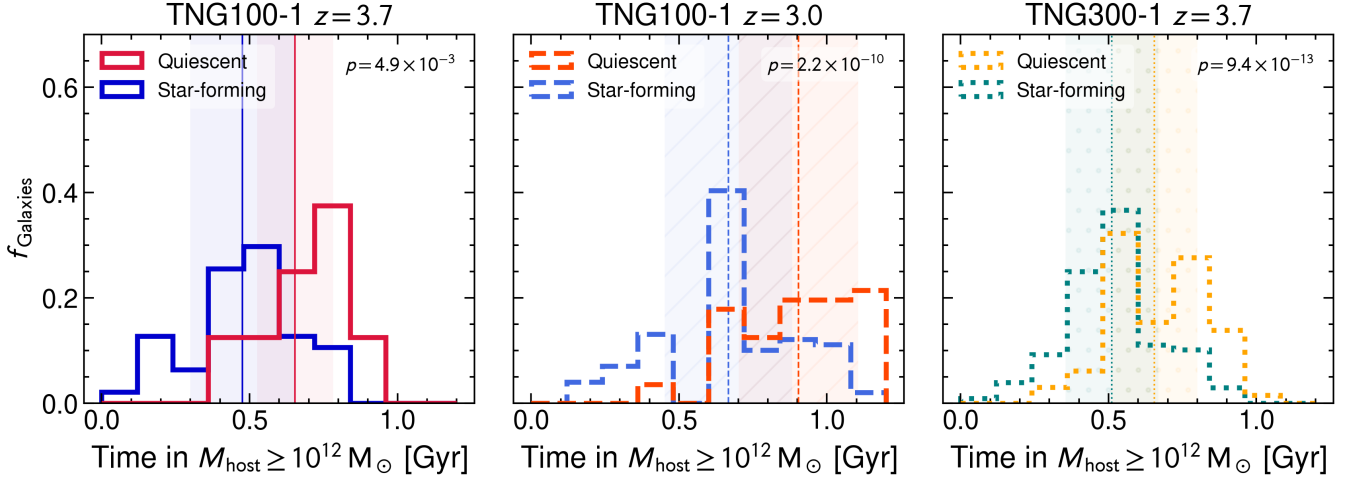


**Figure 5. Impact of Massive Host Halos.** Relative frequency of galaxies with respect to the amount of time that they reside in a “massive host halo”, which we define as halos with a dark matter mass  $\geq 10^{12} M_{\odot}$ . We show separate histograms for the TNG100-1  $z = 3.7$  (left, solid), TNG100-1  $z = 3.0$  (middle, dashed), and TNG300-1  $z = 3.7$  (right, dotted) samples. We also compare the histograms of the quiescent (red shades) and star-forming (blue shades) galaxies in each panel, by indicating their mean-averages (vertical lines) and standard-deviations (translucent box). In each simulation sample, the quiescent galaxies spend more time in a denser environment (i.e. they are hosted in massive halos for longer) than the star-forming galaxies (as also confirmed by the low  $p$ -values from the one-sided T-test of the means, shown in the upper right corners).

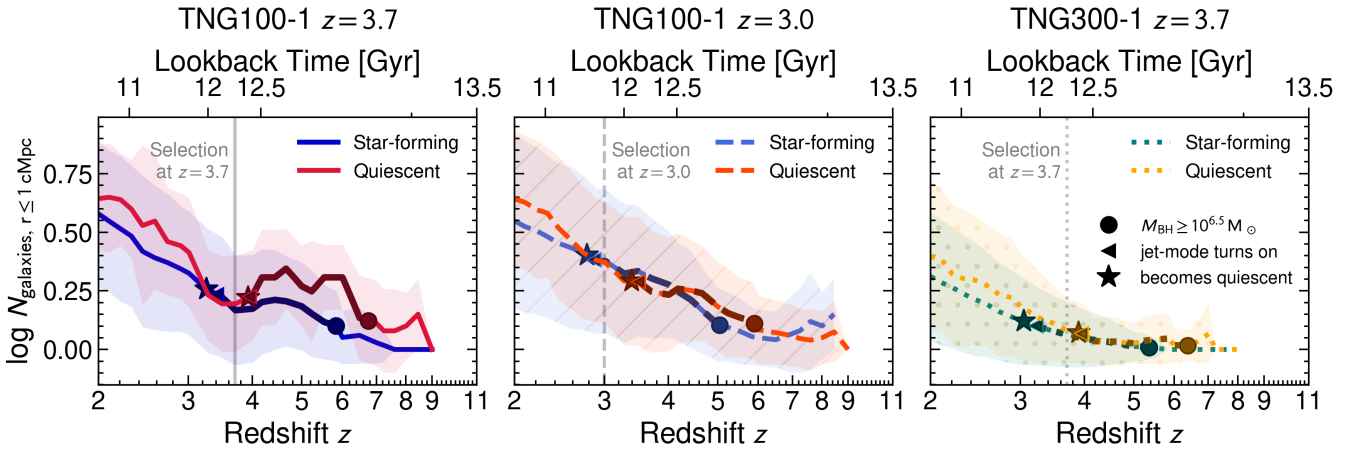


**Figure 6. Environmental Histories.** Redshift evolutions between  $z = 11$  to 2 of the environmental density for the TNG100-1  $z = 3.7$  (left, solid), TNG100-1  $z = 3.0$  (middle, dashed), and TNG300-1  $z = 3.7$  (right, dotted) samples. In each panel, we compare the quiescent (red shades) and star-forming (blue shades) galaxies, by indicating their mean-averaged evolutions and standard-deviations (translucent regions). We also indicate the average period (bolded segments) between when the galaxies’ SMBH masses first exceeded  $10^{6.5} M_{\odot}$  (circle), when their AGN switched to the jet mode (triangle), and the time of quiescence (star). We calculate the environmental density of a galaxy using the number of resolved neighboring subhalos within 1 cMpc. Subhalos are considered to be resolved if they have at least a thousand stellar particles and a thousand dark matter particles. In general, the quiescent galaxies are in slightly more overdense regions. In this way, dense environmental conditions may impact galaxy quenching at high-redshift. The above results appear to be mostly consistent between each simulation sample, except that the TNG300-1 galaxies tend to have lower average densities due to more stringent dark matter and stellar mass cuts.

a contributing factor and mergers do not seem to play any direct role. We now compare our results with those from the literature.

Similar to our work, Hartley et al. (2023) investigate massive galaxy quiescence at  $z \geq 3$  in the TNG300 cosmological simulation. More specifically, they study the time evolution of the first five quenched galaxies that emerge at  $z = 4.2$ . They conclude that AGN feedback has an important contribution to galaxy quenching, especially when enough kinetic energy is released by the AGN. Similarly, we find that the suppression of star formation happens soon after AGN feedback is triggered in the kinetic jet mode. By construction of the AGN feedback model in IllustrisTNG, turning on the jet mode

is only possible when the SMBH reaches a certain mass and when the gas fraction is low enough to prevent further SMBH accretion. This way, the Eddington ratio becomes lower than the empirical quasar-to-jet mode threshold  $\chi$  (see § 2.3). Because the latter scales with the black hole mass squared, this justifies why quenching is favored for fast SMBH growth or, alternatively, for massive SMBHs in the IllustrisTNG simulations (Weinberger et al. 2017; Terrazas et al. 2020; Quai et al. 2021; Park et al. 2022). Other studies also confirm the importance of the low accretion, radiatively inefficient AGN feedback mode in the quenching process in all the IllustrisTNG simulations (Weinberger et al. 2018; Terrazas et al. 2020; Zinger et al.

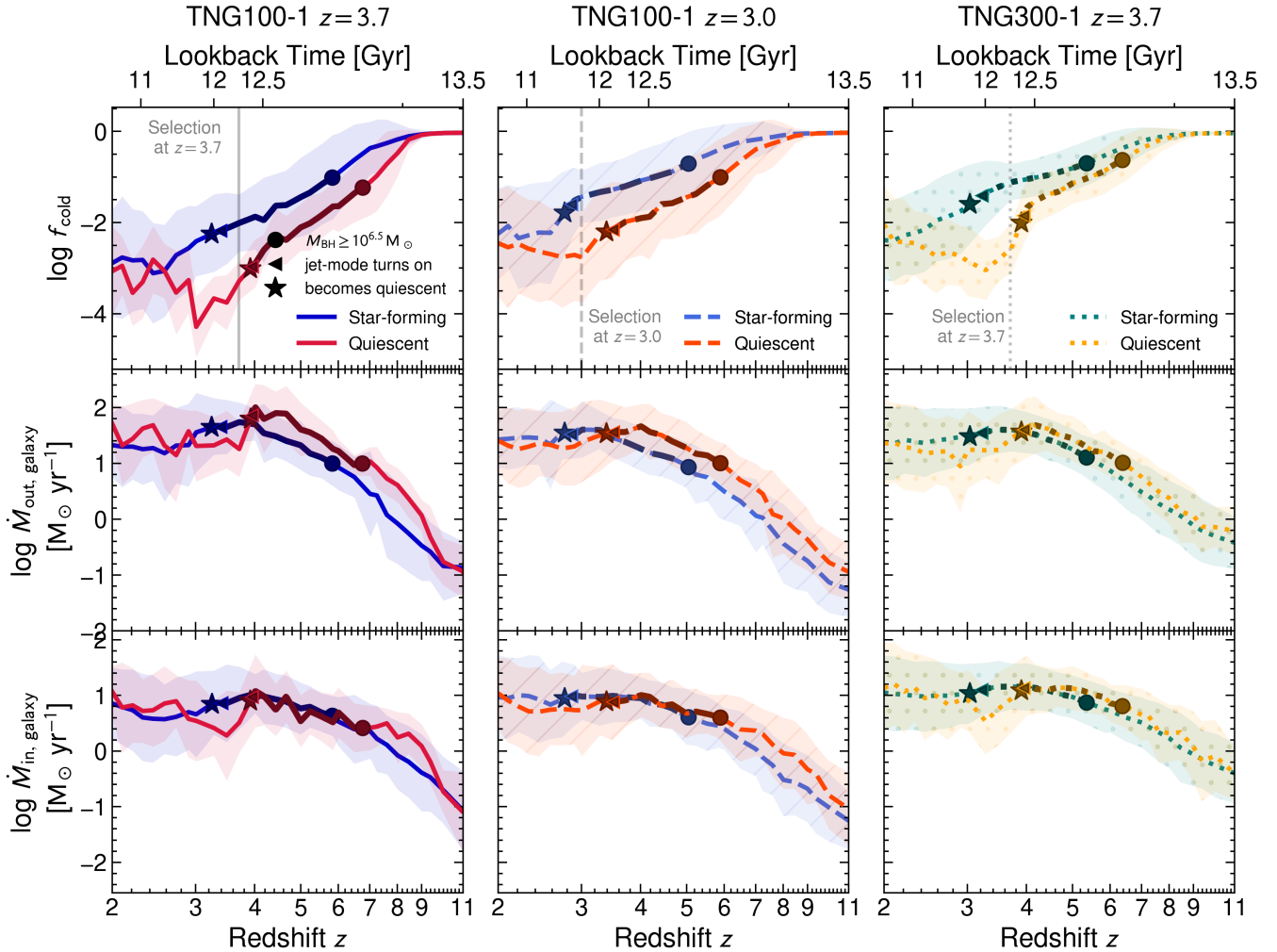


**Figure 7. Gaseous Histories.** Redshift evolutions between  $z = 11$  to 2 of cold gas fraction (top row), gas outflow rate (middle row) and gas inflow rate (bottom row) for the TNG100-1  $z = 3.7$  (left, solid), TNG100-1  $z = 3.0$  (middle, dashed), and TNG300-1  $z = 3.7$  (right, dotted) samples. In each panel, we compare the quiescent (red shades) and star-forming (blue shades) galaxies, by indicating their mean-averaged evolutions and standard-deviations (translucent regions). We also indicate the average period (bolded segments) between when the galaxies’ SMBH masses first exceeded  $10^{6.5} \text{M}_{\odot}$  (circle), when their AGN switched to the jet mode (triangle), and the time of quiescence (star). Gas fractions are measured at twice the stellar half-mass radius, and mass flow rates are measured in spherical shells located at  $R_{\text{galaxy}} = 7R_{\text{eff}}$  (far away enough from the galaxies while still in the circumgalactic medium). Starting at  $z \sim 8$ , the cold gas fraction of the quiescent galaxies begins to decrease below that of the star-forming galaxies. Until their quenching time, quenched galaxies have inflow and outflow rates higher than star-forming galaxies. At the quenching time, quenched galaxies have a small drop in inflow rate and still produce outflows despite a very weak stellar feedback.

2020; Park et al. 2022, 2023), in Simba (Davé et al. 2019), as well as in idealized simulations which use the SWIFT code (Huško et al. 2023). Regardless of the black hole regime, AGN feedback is unambiguously recognized as responsible for galaxy quenching at low redshifts (e.g. Dubois et al. 2016; Beckmann et al. 2017 in Horizon-AGN and Trayford et al. 2016 in EAGLE), and our study indicates that this conclusion is also valid at  $z \geq 3$  (see also Lovell et al. 2023; Lagos et al. 2023).

What remains more debatable is the role of the environment and of the galaxy merger histories. In this work, we find that large-scale environmental conditions play a minor role in quenching, mostly by contributing to stronger accretion rates of dark matter and gas. This 1) impacts black hole seeding, which happens when galaxies are massive enough in the IllustrisTNG simulations, and 2) provides enough gas for the SMBHs to quickly grow and release greater amounts of energy that can in turn impact galaxy growth. The sub-dominance of

the environment in quenching galaxies is also one the main results found by Donnari et al. (2021a): as long as a galaxy is hosted in a massive halo, internal processes such as AGN feedback are responsible for quenching, regardless of the galaxy being a central or satellite. This result, found by analyzing galaxies from TNG100 and TNG300, is mitigated in the smaller volume of the simulation suite. Park et al. (2022) studied  $z = 0$  galaxies with stellar masses  $10^{10.5} - 10^{11.5} \text{M}_{\odot}$  in TNG50 and found that galaxy quenching occurs more rapidly for satellites; a similar finding is stated by Trayford et al. (2016) for the EAGLE simulation. The primary reason is that satellite galaxies are more easily subject to environmental effects, such as ram-pressure stripping and strangulation, that can remove their star-forming gas. We note, however, that our samples of galaxies only contain a few satellites and that the impact of ram-pressure stripping might be more relevant for galaxies less massive than those from our samples (Peng et al. 2015), which we do not investigate in this paper. Eventually,

galaxy mergers are also considered as a channel for galaxy quenching (Man & Belli 2018). After one or several merger events, galaxies can experience a starburst phase before star formation dramatically decreases and all of the gas is consumed. Interestingly, Dubois et al. (2016) note that mergers also induce a peak of AGN activity, which helps to quench galaxies after the burst of star formation. Conversely, when they do not include AGN feedback in the Horizon simulation, the supernova feedback induced after the starburst phase is not sufficient to quench the galaxies. In TNG100, and also at  $z \leq 2$ , Park et al. (2023) show that gas-rich major mergers contribute to galaxy quenching by bringing gas inflows that feed the central SMBH and enhancing its activity. Rodríguez Montero et al. (2019), however, do not find a clear correlation between merger-driven starbursts and galaxy quenching in the Simba simulation, and insist on the role of jet mode AGN feedback instead. In our work, we find very similar merger histories for our quiescent and star-forming samples of galaxies.

Therefore, we do not expect mergers to facilitate quenching at  $z \geq 3$  in TNG100 and TNG300. While the quantitative effect of the environment and of mergers may vary with time and with simulations, the importance of AGN feedback in shutting down star formation in massive galaxies remains to date a consensus in modern simulations, not only at low but also at high redshifts.

### 4.3 Caveats and limitations

To study massive galaxy quenching at high-redshift, we rely on galaxies from the IllustrisTNG simulations at  $z \leq 3.7$ . At this redshift, we consider galaxies as quenched if their sSFR has dropped below  $10^{-10} \text{ yr}^{-1}$  (Franx et al. 2008). In addition, we measure the sSFR within twice the galaxies' stellar half-mass radius, which is closer to what is done in observational works rather than, for example, taking into account all bound stellar particles.<sup>7</sup> As a word of caution, we note that different methods exist to classify populations of observed galaxies (such as using a different sSFR threshold or color-color diagrams) and may lead to different samples of quenched galaxies (see e.g. Donnari et al. 2019, 2021b, with the IllustrisTNG simulations at  $z = 0 - 2$ ).

While there is a growing number of observations showing evidence for galaxy quenching earlier than our target redshift (e.g. Girelli et al. 2019; Nanayakkara et al. 2022; Weaver et al. 2022; Carnall et al. 2023b; Gould et al. 2023; Valentino et al. 2023; Antwi-Danso et al. 2023a), no quiescent galaxies can be found in the TNG100-1 volume beyond  $z = 4.1$  using this definition. The situation gets slightly better in TNG300-1, within which one quiescent galaxy can be found as early as  $z = 4.4$ . However, this remains a poor statistical sample with less galaxies than expected when compared to the number density of massive quiescent galaxies at  $z = 3 - 4$  (Valentino et al. 2023). With JWST, new observations keep pushing the detection of massive quiescent galaxies toward higher redshifts (Carnall et al. 2023b), which poses a strong challenge to all current cosmological simulations to date since they fail in reproducing such rare but existing objects. Therefore, investigating the causes of quenching in the early Universe is currently limited by the ability of numerical simulations to reproduce quenched galaxies at high-redshift. For the last decades, cosmological simulations have been primarily and successfully calibrated to reproduce the properties of local galaxies. In order to make

them better suited to study the complexity of galaxy evolution at early cosmic times, a better understanding and modeling of internal physical processes will be crucial.

In particular, galaxy quenching in simulations is highly related to how black hole growth and feedback are modeled. In the IllustrisTNG simulations, black hole seeding happens above a certain halo mass threshold, and both the seed mass and the halo mass limit are arbitrarily defined to match the  $M_{\text{BH}} - M_{\text{stellar}}$  scaling relation at  $z = 0$  from Kormendy & Ho (2013). EAGLE (Schaye et al. 2015), Horizon-AGN (Dubois et al. 2016), and Simba (Davé et al. 2019) use different black hole seeding prescriptions, but also calibrate their subgrid model to match similar  $z = 0$  scaling relations (e.g. Häring & Rix 2004 for Horizon-AGN and McConnell & Ma 2013 for EAGLE). Currently, the build-up of this relation at high-redshift remains poorly constrained, and all the cosmological simulations aforementioned predict different SMBH and galaxy co-evolution through time. On the one hand, this is because different subgrid models for supernovae and AGN feedback have different efficiencies in regulating galaxy growth, leading to under or over-massive SMBHs compared to their host galaxy masses (Habouzit et al. 2022). On the other hand, this may also be the result of different black hole seeding and growth models. For example, Bennett et al. (2023) recently showed that allowing for earlier black hole seeding and for super-Eddington accretion rates better match the SMBH mass of the brightest high-redshift quasars. The black hole seed mass is especially impactful when SMBH accretion scales with the black hole mass squared, as in the Bondi formalism adopted in most simulations. However, the Bondi formalism is not realistic for the accretion of cold, turbulent gas, which makes up high-redshift galaxies (for more realistic accretion models, see Debuhr et al. 2011; Anglés-Alcázar et al. 2017; Soliman et al. 2023). Together with the precise timing of black hole seeding, the SMBH accretion scheme will determine the timescale for SMBH growth, and, as a consequence, the exposure of the galaxy to AGN feedback.

In this study, we find that the quenching of massive galaxies at high redshifts happens in the IllustrisTNG simulations when the radiatively inefficient AGN feedback mode is turned on. Nevertheless, the transition between the quasar and the jet mode is poorly understood and highly parametrized: it not only depends on the SMBH accretion rate, but also on an empirically motivated black hole pivot mass and Eddington ratio threshold. Although this parametrization contributes to reproducing realistic galaxy populations at  $z = 0$ , it may artificially disfavour the emergence of galaxy quenching at high-redshift. In addition, modeling the quasar mode via isotropic injection of thermal energy has been shown to be barely efficient in regulating star formation (Sijacki et al. 2007; Vogelsberger et al. 2013). Instead, Choi et al. (2015, 2017, 2018) model the broad line absorption winds of AGN in the radiatively efficient regime, which is particularly relevant at high redshifts, and show that this reduces the sSFR and produces more realistic galaxy properties such as X-ray luminosities.

To improve our understanding of how AGN feedback affects star formation, it is necessary to consider other simulations which use different AGN feedback models to realize populations of galaxies. Unlike TNG, not all models use an efficient jet mode, and instead rely on more efficient quasar mode feedback or no jet feedback mode at all to regulate galaxy growth, in an attempt to reproduce realistic galaxy populations (Henden et al. 2018; Schaye et al. 2015; Tremmel et al. 2017). Meanwhile, higher-resolution simulations can better resolve the physical processes resulting from SMBHs at ISM scales (e.g. Wagner & Bicknell 2011; Wagner et al. 2012; Mukherjee et al. 2018; Talbot et al. 2022; Yang & Reynolds 2016; Meece et al. 2017; Bourne

<sup>7</sup> 25% of the TNG100-1  $z = 3.7$  quiescent sample and 52.3% of the TNG300-1  $z = 3.7$  quiescent sample are no longer quiescent when considering all bound particles to determine the sSFR.

& Sijacki 2021; Ehlert et al. 2023). These simulations implement more detailed and physically-motivated prescriptions of thermal and kinetic feedback and can provide different conclusions that may or may not be complementary to the subgrid models of cosmological simulations. We may consider implementing more realistic models for AGN feedback like in zoom-in simulations (Cochrane et al. 2023; Bourne & Sijacki 2017; Rennehan et al. 2023; Huško et al. 2022; Talbot et al. 2024). We also note that in this work, we draw our attention on AGN feedback and did not intend to separate its effect from stellar feedback. Our analysis could also benefit from better prescriptions for stellar feedback and multi-phase ISM modeling, as this can affect the behavior of the central SMBH and how star formation is suppressed (Dubois et al. 2014). To better distinguish their relative effects, an interesting follow-up would consist of re-simulating the massive halos we targeted, similar to the Terrazas et al. (2020) study at  $z = 0$ , with and without the different feedback channels. For instance, turning off the radiatively inefficient AGN feedback mode could confirm its leading role in quenching galaxies.

## 5 CONCLUSION

Using the suite of cosmological simulations IllustrisTNG, we performed an analysis of quiescent, massive galaxies at  $z \gtrsim 3$ . The goal was to understand what suppresses their star formation early in their evolution, and how other similar mass galaxies remain highly star forming. We selected samples of quiescent and star-forming galaxies in three different TNG simulation sets: galaxies from TNG100-1 at  $z = 3.7$  and  $z = 3$ , and from TNG300-1 at  $z = 3.7$ . Our main findings are summarized below:

(i) *There is a clear correlation between galaxy quenching and AGN feedback*: quenched galaxies are exposed for longer to stronger AGN activity than star-forming galaxies. Indeed, leading up to the time of quenching, SMBHs in quenched galaxies accrete at a higher rate and accordingly release larger amounts of thermal energy than those in star-forming galaxies.

(ii) *Galaxies become quenched when the radiatively inefficient kinetic AGN feedback mode is triggered*. Because this happens as soon as the SMBH mass and accretion rate reach a certain threshold, quenching in the TNG simulations is favoured for galaxies whose gas supply enables a fast black hole growth.

(iii) *Large-scale environmental conditions likely contribute to quenching at high-redshift* by enabling the fast and sustained SMBH growth required to trigger AGN feedback in the jet mode. The simulated quiescent galaxies in general reside in more massive host halos and in denser environments throughout their lifetime. As a consequence from their deeper gravitational potential (and likely to their proximity to cosmic filaments), they accrete dark matter and gas at a higher rate than star-forming galaxies, which allows faster stellar mass and black hole growth.

(iv) *Merger events are not important to distinguishing between quiescent and star-forming galaxies* at high redshifts, and are unlikely to favour galaxy quenching at  $z \geq 3$ .

This work gives strong evidence that AGN feedback is the dominant cause of quiescence at high-redshift in the IllustrisTNG simulations. Quenching coincides with the triggering of the kinetic, jet mode AGN feedback when black holes enter the radiatively inefficient regime. For this reason, the precise timing of galaxy quenching is highly dependent on the numerical modeling of AGN feedback, initially tuned so that simulations at  $z = 0$  resemble their observed analogs. As a side effect, massive galaxies do not quench before a

certain time, and cosmological simulations to-date commonly underestimate the number density of massive quenched galaxies at  $z > 3$ . For remedying this issue, one interesting avenue would be to improve our AGN feedback models, especially in the radiatively efficient regime which dominates at early cosmic epochs. This would help a better understanding of the role of AGN feedback in quenching galaxies, from the cosmic dawn to present-day.

## DATA AVAILABILITY

Data directly related to the figures of this publication are available on request from SK. The IllustrisTNG simulations are publicly available at [www.tng-project.org/data](http://www.tng-project.org/data) (Nelson et al. 2019).

## ACKNOWLEDGEMENTS

The authors would like to thank the referees for useful comments in the revision of this manuscript. SK acknowledges support from the U.S. Fulbright Scholarship program at the time of completing this work, and is thankful to Annalisa Pillepich for insightful conversations as well as the opportunity to present the results at the GASPISA2024—“The Physical Processes Shaping the Stellar and Gaseous Histories of Galaxies”—conference. MH and MF acknowledge funding from the Swiss National Science Foundation (SNF) via a PRIMA Grant PR00P2 193577 “From Cosmic Dawn to High Noon: The Role of Black Holes for Young Galaxies.” FV at is funded by the Danish National Research Foundation under Grant No. 140.

## REFERENCES

- Anglés-Alcázar D., Davé R., Faucher-Giguère C.-A., Özel F., Hopkins P. F., 2017, *MNRAS*, **464**, 2840
- Antwi-Danso J., et al., 2023a, [arXiv e-prints](https://arxiv.org/abs/2307.09590), p. arXiv:2307.09590
- Antwi-Danso J., et al., 2023b, *ApJ*, **943**, 166
- Arav N., Borguet B., Chamberlain C., Edmonds D., Danforth C., 2013, *MNRAS*, **436**, 3286
- Beckmann R. S., et al., 2017, *MNRAS*, **472**, 949
- Bennett J. S., Sijacki D., Costa T., Laporte N., Witten C., 2023, [arXiv e-prints](https://arxiv.org/abs/2305.11932), p. arXiv:2305.11932
- Bocquet S., Saro A., Dolag K., Mohr J. J., 2016, *MNRAS*, **456**, 2361
- Book L. G., Benson A. J., 2010, *ApJ*, **716**, 810–818
- Boselli A., et al., 2016, *A&A*, **596**, A11
- Bourne M. A., Sijacki D., 2017, *MNRAS*, **472**, 4707
- Bourne M. A., Sijacki D., 2021, *MNRAS*, **506**, 488
- Bower R. G., Benson A. J., Malbon R., Helly J. C., Frenk C. S., Baugh C. M., Cole S., Lacey C. G., 2006, *MNRAS*, **370**, 645
- Cano-Díaz M., Maiolino R., Marconi A., Netzer H., Shemmer O., Cresci G., 2012, *A&A*, **537**, L8
- Carnall A. C., et al., 2023a, *MNRAS*, **520**, 3974
- Carnall A. C., et al., 2023b, *Nature*, **619**, 716
- Cecchi R., Bolzonella M., Cimatti A., Girelli G., 2019, *ApJ*, **880**, L14
- Chevalier R. A., Clegg A. W., 1985, *Nature*, **317**, 44
- Choi E., Ostriker J. P., Naab T., Oser L., Moster B. P., 2015, *MNRAS*, **449**, 4105
- Choi E., Ostriker J. P., Naab T., Somerville R. S., Hirschmann M., Núñez A., Hu C.-Y., Oser L., 2017, *ApJ*, **844**, 31
- Choi E., Somerville R. S., Ostriker J. P., Naab T., Hirschmann M., 2018, *ApJ*, **866**, 91
- Cicone C., et al., 2014, *A&A*, **562**, A21
- Ciotti L., D’Ercole A., Pellegrini S., Renzini A., 1991, *ApJ*, **376**, 380
- Cochrane R. K., et al., 2023, *MNRAS*, **523**, 2409

- Costa T., Rosdahl J., Sijacki D., Haehnelt M. G., 2018, *MNRAS*, **479**, 2079
- Croton D. J., et al., 2006, *MNRAS*, **365**, 11
- Davé R., Anglés-Alcázar D., Narayanan D., Li Q., Rafieferantsoa M. H., Appleby S., 2019, *MNRAS*, **486**, 2827
- Debuhr J., Quataert E., Ma C.-P., 2011, *MNRAS*, **412**, 1341
- Di Matteo T., Springel V., Hernquist L., 2005, *Nature*, **433**, 604
- Donnari M., et al., 2019, *MNRAS*, **485**, 4817
- Donnari M., et al., 2021a, *MNRAS*, **500**, 4004
- Donnari M., Pillepich A., Nelson D., Marinacci F., Vogelsberger M., Hernquist L., 2021b, *MNRAS*, **506**, 4760
- Dubois Y., Devriendt J., Slyz A., Teyssier R., 2012, *MNRAS*, **420**, 2662
- Dubois Y., Volonteri M., Silk J., Devriendt J., Slyz A., 2014, *MNRAS*, **440**, 2333
- Dubois Y., Peirani S., Pichon C., Devriendt J., Gavazzi R., Welker C., Volonteri M., 2016, *MNRAS*, **463**, 3948
- Ehler K., Weinberger R., Pfrommer C., Pakmor R., Springel V., 2023, *MNRAS*, **518**, 4622
- Fabian A. C., 2012, *ARA&A*, **50**, 455
- Faucher-Giguère C.-A., Quataert E., 2012, *MNRAS*, **425**, 605
- Feruglio C., Maiolino R., Piconcelli E., Menci N., Aussel H., Lamastra A., Fiore F., 2010, *A&A*, **518**, L155
- Fischer J., et al., 2010, *A&A*, **518**, L41
- Forrest B., et al., 2020, *ApJ*, **903**, 47
- Förster Schreiber N. M., et al., 2014, *ApJ*, **787**, 38
- Franx M., van Dokkum P. G., Förster Schreiber N. M., Wuyts S., Labbé I., Toft S., 2008, *ApJ*, **688**, 770
- Genel S., et al., 2014, *MNRAS*, **445**, 175
- Genzel R., et al., 2014, *ApJ*, **796**, 7
- Girelli G., Bolzonella M., Cimatti A., 2019, *A&A*, **632**, A80
- Gould K. M. L., et al., 2023, *AJ*, **165**, 248
- Habouzit M., et al., 2022, *MNRAS*, **511**, 3751
- Hardcastle M., 2018, *Nature Astronomy*, **2**, 273
- Hardcastle M. J., Croston J. H., 2020, *New Astron. Rev.*, **88**, 101539
- Häring N., Rix H.-W., 2004, *ApJ*, **604**, L89
- Harrison C. M., Alexander D. M., Mullaney J. R., Swinbank A. M., 2014, *MNRAS*, **441**, 3306
- Harrison C. M., et al., 2015, *MNRAS*, **456**, 1195
- Hartley A. I., et al., 2023, *MNRAS*, **522**, 3138
- Henden N. A., Puchwein E., Shen S., Sijacki D., 2018, *MNRAS*, **479**, 5385
- Hirschmann M., Dolag K., Saro A., Bachmann L., Borgani S., Burkert A., 2014a, *MNRAS*, **442**, 2304
- Hirschmann M., De Lucia G., Wilman D., Weinmann S., Iovino A., Cucciati O., Zibetti S., Villalobos Á., 2014b, *MNRAS*, **444**, 2938
- Huško F., Lacey C. G., Schaye J., Schaller M., Nobels F. S. J., 2022, *MNRAS*, **516**, 3750
- Huško F., Lacey C. G., Schaye J., Nobels F. S. J., Schaller M., 2023, *arXiv e-prints*, p. [arXiv:2307.01409](https://arxiv.org/abs/2307.01409)
- Ishibashi W., Fabian A. C., 2012, *MNRAS*, **427**, 2998
- Ishibashi W., Fabian A. C., 2015, *MNRAS*, **451**, 93
- Khochfar S., Ostriker J. P., 2008, *ApJ*, **680**, 54
- King A., Pounds K., 2015, *ARA&A*, **53**, 115
- Kormendy J., Ho L. C., 2013, *ARA&A*, **51**, 511
- Kravtsov A. V., 2013, *ApJ*, **764**, L31
- Lagos C. D. P., et al., 2023, *arXiv e-prints*, p. [arXiv:2309.02310](https://arxiv.org/abs/2309.02310)
- Long A. S., et al., 2023, *arXiv e-prints*, p. [arXiv:2305.04662](https://arxiv.org/abs/2305.04662)
- Lovell C. C., et al., 2023, *MNRAS*, **525**, 5520
- Man A., Belli S., 2018, *Nature Astronomy*, **2**, 695
- Marinacci F., et al., 2018, *MNRAS*, **480**, 5113
- McConnell N. J., Ma C.-P., 2013, *ApJ*, **764**, 184
- Meece G. R., Voit G. M., O’Shea B. W., 2017, *ApJ*, **841**, 133
- Merlin E., et al., 2019, *MNRAS*, **490**, 3309–3328
- Mihos J. C., Hernquist L., 1996, *ApJ*, **464**, 641
- Mukherjee D., Bicknell G. V., Wagner A. Y., Sutherland R. S., Silk J., 2018, *MNRAS*, **479**, 5544
- Naiman J. P., et al., 2018, *MNRAS*, **477**, 1206
- Nanayakkara T., et al., 2022, *arXiv e-prints*, p. [arXiv:2212.11638](https://arxiv.org/abs/2212.11638)
- Nelson D., et al., 2018, *MNRAS*, **475**, 624
- Nelson D., et al., 2019, *Computational Astrophysics and Cosmology*, **6**, 2
- Oser L., Ostriker J. P., Naab T., Johansson P. H., Burkert A., 2010, *ApJ*, **725**, 2312
- Park M., et al., 2022, *MNRAS*, **515**, 213
- Park M., et al., 2023, *ApJ*, **953**, 119
- Peng Y., Maiolino R., Cochrane R., 2015, *Nature*, **521**, 192–195
- Pillepich A., et al., 2017, *MNRAS*, **473**, 4077–4106
- Pillepich A., et al., 2018, *MNRAS*, **475**, 648
- Quai S., Hani M. H., Ellison S. L., Patton D. R., Woo J., 2021, *MNRAS*, **504**, 1888
- Ramesh R., Nelson D., Pillepich A., 2023, *MNRAS*, **518**, 5754
- Rees M. J., Ostriker J. P., 1977, *MNRAS*, **179**, 541
- Rennehan D., Babul A., Moa B., Davé R., 2023, *arXiv e-prints*, p. [arXiv:2309.15898](https://arxiv.org/abs/2309.15898)
- Rodriguez-Gomez V., et al., 2015, *MNRAS*, **449**, 49–64
- Rodríguez Montero F., Davé R., Wild V., Anglés-Alcázar D., Narayanan D., 2019, *MNRAS*, **490**, 2139
- Rupke D. S. N., Veilleux S., 2013, *ApJ*, **768**, 75
- Santini P., et al., 2021, *A&A*, **652**, A30
- Schaye J., et al., 2015, *MNRAS*, **446**, 521
- Schreiber C., et al., 2018, *A&A*, **618**, A85
- Schreiber N. M. F., et al., 2019, *ApJ*, **875**, 21
- Sijacki D., Springel V., Di Matteo T., Hernquist L., 2007, *MNRAS*, **380**, 877
- Sijacki D., Vogelsberger M., Genel S., Springel V., Torrey P., Snyder G. F., Nelson D., Hernquist L., 2015, *MNRAS*, **452**, 575–596
- Smethurst R. J., Lintott C. J., Bamford S. P., Hart R. E., Kruk S. J., Masters K. L., Nichol R. C., Simmons B. D., 2017, *MNRAS*, **469**, 3670–3687
- Soliman N. H., Macciò A. V., Blank M., 2023, *MNRAS*, **525**, 12
- Somerville R. S., Hopkins P. F., Cox T. J., Robertson B. E., Hernquist L., 2008, *MNRAS*, **391**, 481
- Somerville R. S., et al., 2018, *MNRAS*, **473**, 2714
- Springel V., 2010, *MNRAS*, **401**, 791
- Springel V., Hernquist L., 2003, *MNRAS*, **339**, 289
- Springel V., White S. D. M., Tormen G., Kauffmann G., 2001, *MNRAS*, **328**, 726
- Springel V., Di Matteo T., Hernquist L., 2005, *MNRAS*, **361**, 776
- Springel V., et al., 2018, *MNRAS*, **475**, 676
- Sturm E., et al., 2011, *ApJ*, **733**, L16
- Talbot R. Y., Sijacki D., Bourne M. A., 2022, *MNRAS*, **514**, 4535
- Talbot R. Y., Sijacki D., Bourne M. A., 2024, *MNRAS*, **528**, 5432
- Terrazas B. A., Bell E. F., Woo J., Henriques B. M. B., 2017, *ApJ*, **844**, 170
- Terrazas B. A., et al., 2020, *MNRAS*, **493**, 1888
- Thompson T. A., Fabian A. C., Quataert E., Murray N., 2015, *MNRAS*, **449**, 147
- Torrey P., et al., 2019, *MNRAS*
- Trayford J. W., Theuns T., Bower R. G., Crain R. A., Lagos C. d. P., Schaller M., Schaye J., 2016, *MNRAS*, **460**, 3925
- Tremmel M., Karcher M., Governato F., Volonteri M., Quinn T. R., Pontzen A., Anderson L., Bellovary J., 2017, *MNRAS*, **470**, 1121
- Valentino F., et al., 2020, *ApJ*, **889**, 93
- Valentino F., et al., 2023, *ApJ*, **947**, 20
- Vogelsberger M., Genel S., Sijacki D., Torrey P., Springel V., Hernquist L., 2013, *MNRAS*, **436**, 3031
- Vogelsberger M., et al., 2014, *MNRAS*, **444**, 1518
- Vogelsberger M., et al., 2018, *MNRAS*, **474**, 2073–2093
- Wagner A. Y., Bicknell G. V., 2011, *ApJ*, **728**, 29
- Wagner A. Y., Bicknell G. V., Umemura M., 2012, *ApJ*, **757**, 136
- Weaver J. R., et al., 2022, *arXiv e-prints*, p. [arXiv:2212.02512](https://arxiv.org/abs/2212.02512)
- Weinberger R., et al., 2017, *MNRAS*, **465**, 3291
- Weinberger R., et al., 2018, *MNRAS*, **479**, 4056
- Westmoquette M. S., Clements D. L., Bendo G. J., Khan S. A., 2012, *MNRAS*, **424**, 416
- Wetzel A. R., Tinker J. L., Conroy C., van den Bosch F. C., 2013, *MNRAS*, **432**, 336
- Yang H. Y. K., Reynolds C. S., 2016, *ApJ*, **829**, 90
- Zinger E., et al., 2020, *MNRAS*, **499**, 768

This paper has been typeset from a  $\text{\TeX}/\text{\LaTeX}$  file prepared by the author.